
Nested Optimal Transport Distances

Ruben Bontorno

Department of Mathematics
ETH Zürich

rbontorno@student.ethz.ch

Songyan Hou

Department of Mathematics
ETH Zürich

songyan.hou@math.ethz.ch

Abstract

Simulating realistic financial time series is essential for stress testing, scenario generation, and decision-making under uncertainty. Despite advances in deep generative models, there is no consensus metric for their evaluation. We focus on generative AI for financial time series in decision-making applications and employ the *nested optimal transport distance*—a time-causal variant of optimal transport distance, which is robust to tasks such as hedging, optimal stopping, and reinforcement learning. Moreover, we propose a statistically consistent, naturally parallelizable algorithm for its computation, achieving substantial speedups over existing approaches.

1 Introduction

Recent advances in generative AI have opened new frontiers for applications in finance, such as financial modeling, stress testing, scenario generation, automated financial services, and decision-making under uncertainty; see [1, 2]. The goal of generative AI is to generate synthetic financial data “indistinguishable” from real financial data, and the “indistinguishability” are evaluated by probabilistic metrics. Due to the unique characteristics in different applications of generated financial data, it is natural to expect no consensus metrics like FID (Fréchet Inception Distance) in image generation evaluation. But the lack of even an intra-application consensus-metric makes it difficult to compare different models [3]. A qualified consensus-metric is supposed to satisfy the following two criteria: robustness and tractability.

Robustness: The consensus-metric should robustly control a basket of quantities of interest.

Tractability: The metric should be computationally tractable with samples.

A large class of generative AI models for financial time series is trained for decision-making applications, including dynamic hedging, optimal stopping, utility maximization, and reinforcement learning. Notably, these problems are not continuous with respect to widely-used distances, such as the Maximum Mean Discrepancy (MMD) and the Wasserstein distances (\mathcal{W} -distances). However, these problems are Lipschitz-continuous with respect to stronger metrics, called adapted Wasserstein distances (\mathcal{AW} -distances), also known as nested Wasserstein distances, which have been introduced as a variant of \mathcal{W} -distances that accounts for the time-causal structure of stochastic processes. \mathcal{AW} -distances serve as robust distances for many dynamic stochastic optimization problems across several fields, particularly in mathematical finance and economics; see [4–7]. Therefore, for robustness purposes, it is desirable to evaluate the generated time series distribution under \mathcal{AW} -distances.

While \mathcal{AW} -distances ensure robustness, the existing implementation calculating \mathcal{AW} -distances are slow and does not scale to long time series (see implementations in [8–10]). In this paper, we propose a natural parallelization algorithm to calculate \mathcal{AW} -distances, which achieves orders-of-magnitude speedups over existing implementations and also behaves statistically consistently.

2 Nested optimal transport distances

We regard \mathbb{R}^{dT} as the space of d -dimensional discrete-time paths with T time steps. Notation follows standard conventions and is intended to be self-explanatory; further details or clarifications of notations are provided in Appendix A.1.

Definition 1. For $\mu, \nu \in \mathcal{P}_2(\mathbb{R}^{dT})$, the Wasserstein-2 distance $\mathcal{W}_2(\cdot, \cdot)$ on $\mathcal{P}_2(\mathbb{R}^{dT})$ is defined by

$$\mathcal{W}_2^2(\mu, \nu) := \inf_{\pi \in \text{Cpl}(\mu, \nu)} \int \|x - y\|^2 \pi(dx, dy), \quad (1)$$

where $\text{Cpl}(\mu, \nu)$ denotes the set of couplings between μ and ν , that is, probabilities in $\mathcal{P}(\mathbb{R}^{dT} \times \mathbb{R}^{dT})$ with first marginal μ and second marginal ν .

Next, we restrict our attention to couplings $\pi \in \text{Cpl}(\mu, \nu)$ such that the conditional law of π is still a coupling of the conditional laws of μ and ν , that is for all $t = 0, \dots, T-1$, $\pi_{x_{1:t}, y_{1:t}} \in \text{Cpl}(\mu_{x_{1:t}}, \nu_{y_{1:t}})$. Such couplings are called bi-causal, and denoted by $\text{Cpl}_{bc}(\mu, \nu)$.

Definition 2. For $\mu, \nu \in \mathcal{P}_2(\mathbb{R}^{dT})$, the adapted Wasserstein-2 distance $\mathcal{AW}_2(\cdot, \cdot)$ on $\mathcal{P}(\mathbb{R}^{dT})$ is defined by

$$\mathcal{AW}_2^2(\mu, \nu) := \inf_{\pi \in \text{Cpl}_{bc}(\mu, \nu)} \int \sum_{t=1}^T \|x_t - y_t\|^2 \pi(dx, dy). \quad (2)$$

The adaptedness (or bi-causality) imposed on couplings modifies the Wasserstein distance to ensure robustness of a large class of “well-defined” dynamic optimization problems, ranging from optimal stopping and utility maximization to dynamic risk minimization and dynamic hedging; see [5–7, 11–13]. We therefore present only the general statement here, while providing illustrative examples in the appendix and referring the reader to the cited references for further details.

Robustness ([7, 11–13]). Let $\mu, \nu \in \mathcal{P}_2(\mathbb{R}^{dT})$ and $v: \mathcal{P}_2(\mathbb{R}^{dT}) \rightarrow \mathbb{R}$, where $v(\mu)$ denotes the optimal value of a “well-defined” dynamic optimization problem under μ . Then under “mild conditions”, there exists $L \geq 0$ such that the following holds

$$|v(\mu) - v(\nu)| \leq L \mathcal{AW}_2(\mu, \nu).$$

From the perspective of nested disintegration, Pflug-Pichler define the adapted Wasserstein distance as nested distance in [11] and establish an alternative representation of $\mathcal{AW}_2(\cdot, \cdot)$ through the dynamic programming principle; see the proof of Proposition 1 in Appendix A.3.

Proposition 1 (Dynamic programming principle). Let $\mu, \nu \in \mathcal{P}_2(\mathbb{R}^{dT})$. Set $V_T^{\mu, \nu} \equiv 0$ and define for all $t = 0, \dots, T-1$,

$$V_t^{\mu, \nu}(x_{1:t}, y_{1:t}) = \inf_{\pi_{x_{1:t}, y_{1:t}}^{t+1} \in \text{Cpl}_{bc}(\mu_{x_{1:t}}^{t+1}, \nu_{y_{1:t}}^{t+1})} \int \left[\|x_{t+1} - y_{t+1}\|^2 + V_{t+1}^{\mu, \nu}(x_{1:t+1}, y_{1:t+1}) \right] d\pi_{x_{1:t}, y_{1:t}}^{t+1}.$$

Then for all $t = 0, \dots, T-1$, $V_t^{\mu, \nu}(x_{1:t}, y_{1:t}) = \mathcal{AW}_2^2(\mu_{x_{1:t}}, \nu_{y_{1:t}})$ and $V_0^{\mu, \nu} \equiv \mathcal{AW}_2^2(\mu, \nu)$.

The computation of $V_t^{\mu, \nu}(x_{1:t}, y_{1:t})$ can be fully parallelized over all admissible pairs $(x_{1:t}, y_{1:t})$, which is the key reason why our algorithm is naturally parallel. Before detailing our algorithm, we need to introduce *adapted empirical measures*, originally proposed in [14] to address the statistical estimation problem for \mathcal{AW} -distances.

Definition 3. Let $N \in \mathbb{N}$ be the number of samples and $\Delta_N > 0$. We tile \mathbb{R}^{dT} with cubes with edges of length Δ_N and let φ^N map each such small cube to its center. For $\mu \in \mathcal{P}_1(\mathbb{R}^{dT})$, we let $(x^{(n)})_{n \in \mathbb{N}}$ be i.i.d. samples from μ . Then we define $\hat{\mu}^N = \sum_{i=1}^N \delta_{\varphi^N(x^{(i)})}$ and call $\hat{\mu}^N$ the adapted empirical measures of μ .

For \mathcal{AW} -distances, empirical measures fail to converge, but adapted empirical measures converge to the underlying measure as the number of samples N goes to infinity, which provides statistical guarantee approximating μ with $\hat{\mu}^N$ in calculating \mathcal{AW} -distances; see the proof of Theorem 2 in Appendix A.3.

Theorem 2. Let $\mu \in \mathcal{P}_2(\mathbb{R}^{dT})$ and $\Delta_N = N^{-\frac{1}{dT}}$. Then $\lim_{N \rightarrow \infty} \mathcal{AW}_2(\mu, \hat{\mu}^N) = 0$ almost surely.

Parallel computing algorithm: We now introduce our algorithm, which consists of two main steps: *quantization* and *backward computation*. In the first quantization step, we fix Δ_N and map each sample $x^{(i)} \in \mathbb{R}^{dT}$ to its quantized counterpart $q^{(i)} := \varphi^N(x^{(i)})$ on lattice. Since the quantized samples lie on a lattice in \mathbb{R}^{dT} , if N is sufficiently large, multiple quantized samples coincide up to time t , hereby endowing $\hat{\mu}^N$ a tree structure; see visualization in Figure 2. In the second backward computation step, we first leverage this tree structure and compute the conditional distribution:

$$(\hat{\mu}^N)_{q_{1:t}}^{t+1} = \frac{1}{|\mathcal{I}_{q_{1:t}}|} \sum_{i \in \mathcal{I}_{q_{1:t}}} \delta_{q_{t+1}^{(i)}}, \quad \mathcal{I}_{q_{1:t}} = \{i \leq N \mid q_{1:t}^{(i)} = q_{1:t}\}, \quad q_{1:t} \in \{q_{1:t}^{(i)} \mid i \leq N\}.$$

Once $(\hat{\mu}^N)_{q_{1:t}}^{t+1}$ and $(\hat{\nu}^N)_{q_{1:t}}^{t+1}$ have been computed, we can apply the dynamic programming principle to compute $V_t^{\hat{\mu}^N, \hat{\nu}^N}$ backward, continuing until we reach $V_0^{\hat{\mu}^N, \hat{\nu}^N}$, which equals $\mathcal{AW}_2^2(\hat{\mu}^N, \hat{\nu}^N)$ by Proposition 1. Finally, by Theorem 2, $\mathcal{AW}_2^2(\hat{\mu}^N, \hat{\nu}^N)$ converges to $\mathcal{AW}_2^2(\mu, \nu)$.

Markovian improvement: In general, the moment convergence rate of \mathcal{AW}_2 : $\mathbb{E}[\mathcal{AW}_2(\mu, \hat{\mu}^N)] = O(N^{-\frac{1}{dT}})$; see [14, Theorem 1.5] suffers from the same curse of dimensionality as \mathcal{W}_2 ; see [15, Theorem 1]. This significantly restricts its applicability to long time series, even in the univariate case. However, if μ is known to be Markovian, there is a natural Markovian modification of the adapted empirical measure, simply replacing $(\hat{\mu}^N)_{q_{1:t}}^{t+1}$ by $(\hat{\mu}^N)_{q_t}^{t+1}$, which can be similarly defined as $(\hat{\mu}^N)_{q_{1:t}}^{t+1}$; see [14]. This modification yields substantially improved statistical convergence rates $O(N^{-\frac{1}{2d}})$ that are independent of T ; see Theorem 6.1 in [14]. In addition, the Markovian modification significantly reduces the computational time in practice.

3 Numerical experiments

For Gaussian distributions, explicit closed-form expressions exist for both the \mathcal{AW}_2 and \mathcal{W}_2 distances (see Appendix A.4). We assess the convergence of our algorithm by benchmarking against these closed forms. All experiments were conducted on an AMD EPYC 7763 processor (64 cores, 2.45 GHz).

Ornstein-Uhlenbeck processes. Let us first consider the Ornstein-Uhlenbeck (OU) processes $X^\sigma = (X_t^\sigma)_{t \geq 0}$, defined by

$$dX_t^\sigma = -X_t^\sigma dt + \sigma dW_t, \quad X_0 = 0,$$

where $(W_t)_{t \geq 0}$ is a Brownian motion and $\sigma \in \mathbb{R}_+$. Let $N = 5$, $\Delta t = 1/N$, and consider $\tilde{X}_{1:N}^\sigma := [X_{\Delta t}^\sigma, \dots, X_{N\Delta t}^\sigma]$. Denoting by μ^σ the distribution of $\tilde{X}_{1:N}^\sigma$, we compute $\mathcal{AW}_2^2(\mu^1, \mu^3)$ with randomly generated i.i.d. samples using the Markovian implementation of our algorithm, and evidently, numerical values of \mathcal{AW}_2^2 converge to its theoretical value; see Figure 1.

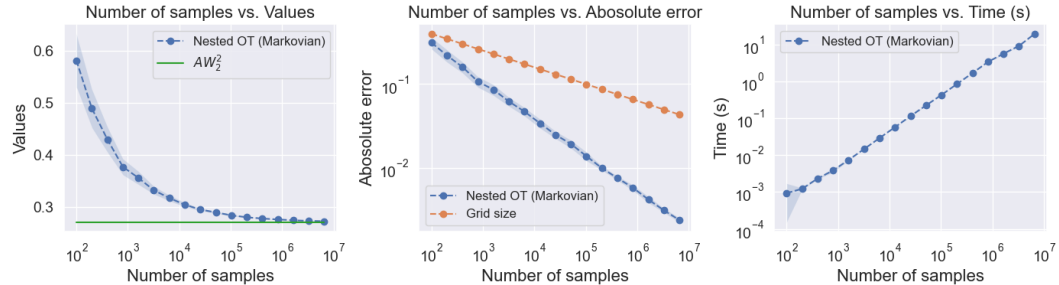


Figure 1: Numerical optimal values, absolute errors, and runtimes for \mathcal{AW}_2^2 with Markovian implementation across different sample sizes (averaged over 10 independent runs per sample size).

Fake Brownian Motion. Let $(W_t)_{t \in [0,1]}$ be a Brownian motion, $Z \sim \mathcal{N}(0, 1)$ independent of $(W_t)_{t \in [0,1]}$ and $\delta \in (0, 1)$. Now, we define a *fake Brownian motion* $X = (X_t)_{t \in [0,1]}$ such that

$$X_t = \begin{cases} W_t + \frac{t-\delta}{1-\delta}(Z - W_1) + \frac{1-t}{1-\delta}(\sqrt{\delta}Z - W_\delta), & t \in [\delta, 1], \\ \frac{t}{\sqrt{\delta}}Z, & t \in [0, \delta]. \end{cases}$$

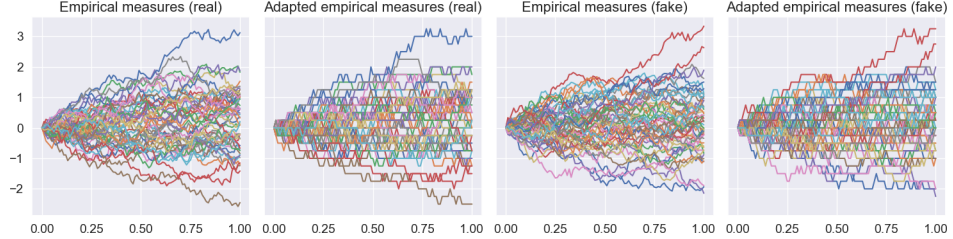


Figure 2: Visualization of empirical measures and adapted empirical measures with 50 samples for real Brownian motion $(W_t)_{t \geq 0}$ and fake Brownian motion $(X_t)_{t \geq 0}$.

The process X is called “fake” because, for small δ , its sample paths are visually indistinguishable from those of Brownian motion; see visualization in Figure 2. However, X is not a Brownian motion since it satisfies $X_\delta = \sqrt{\delta} X_1$, meaning that X_1 is perfectly predictable at time δ from the observation of X_δ . If we interpret X and W as asset price processes, they exhibit fundamentally different behaviors: the simple strategy of going long on X when $X_\delta > 0$ and short on X when $X_\delta < 0$ yields arbitrage opportunities, whereas trading solely in W is arbitrage-free.

Consider the marginal $X_{\delta,t,1} := [X_\delta, X_t, X_1]^\top$, where $0 < \delta < t < 1$, which satisfies that

$$X_{\delta,t,1} = L_{\delta,t} \begin{bmatrix} Z \\ \frac{W_t}{\sqrt{t}} \\ \frac{W_1 - W_t}{\sqrt{1-t}} \end{bmatrix}, \quad L_{\delta,t} = \begin{bmatrix} \sqrt{\delta} & 0 & 0 \\ \frac{t-\delta+(1-t)\sqrt{\delta}}{1-\delta} & \frac{(1-t)(t-\delta)}{\sqrt{t}(1-\delta)} & 0 \\ 1 & 0 & 0 \end{bmatrix}.$$

We denote by $\mu_{\delta,t,1}^X$ the distribution of $X_{\delta,t,1}$ and by $\mu_{\delta,t,1}^W$ the distribution of $W_{\delta,t,1} := [W_\delta, W_t, W_1]^\top$. For $\delta = 0.1$ and $t = 0.5$, we compute $\mathcal{AW}_2^2(\mu_{\delta,t,1}^X, \mu_{\delta,t,1}^W)$ and $\mathcal{W}_2^2(\mu_{\delta,t,1}^X, \mu_{\delta,t,1}^W)$ numerically, and compare them with their corresponding theoretical values, calculated by (3) and (4); see Figure 3. Evidently, numerical values of \mathcal{AW}_2^2 and \mathcal{W}_2^2 converge to their theoretical values, respectively, but $\mu_{\delta,t,1}^X$ and $\mu_{\delta,t,1}^W$ are only well-distinguished by \mathcal{AW}_2^2 and not by \mathcal{W}_2^2 . The values of \mathcal{AW}_2^2 are computed with non-Markovian implementation of our algorithm with PNOT: Python Nested Optimal Transport since $X_{\delta,t,1}$ is not Markovian, and those of \mathcal{W}_2^2 are computed with POT: Python Optimal Transport [16].

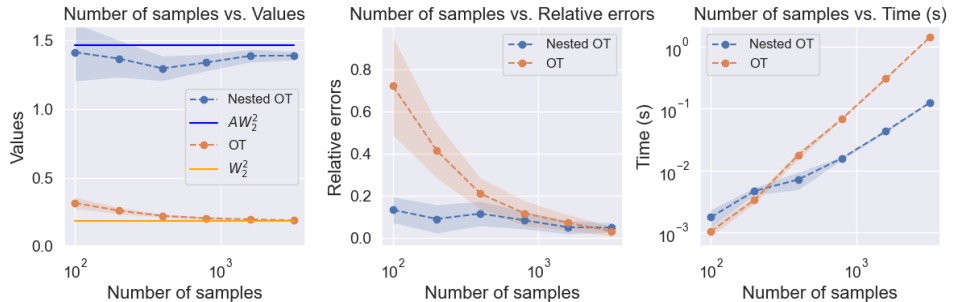


Figure 3: Numerical optimal values, absolute errors, and runtimes for \mathcal{AW}_2^2 and \mathcal{W}_2^2 across different sample sizes (averaged over 10 independent runs per sample size). The \mathcal{AW}_2^2 is calculated with our algorithm with non-Markovian implementation and the \mathcal{W}_2^2 is calculated by `ot.lp.emd` (POT).

4 Conclusion

In this work, we highlight the lack of a consensus metric for evaluating generative AI in financial time series and propose the nested optimal transport. To address the computational challenges of this metric, we develop a naturally parallelizable algorithm that enables substantial speedups over existing methods. Our approach is theoretically supported by statistical analysis and empirically validated through numerical experiments.

References

- [1] Samuel A Assefa, Danial Dervovic, Mahmoud Mahfouz, Robert E Tillman, Prashant Reddy, and Manuela Veloso. Generating synthetic data in finance: opportunities, challenges and pitfalls. In *Proceedings of the First ACM International Conference on AI in Finance*, pages 1–8, 2020.
- [2] Lars Ericson, Xuejun Zhu, Xusi Han, Rao Fu, Shuang Li, Steve Guo, and Ping Hu. Deep generative modeling for financial time series with application in var: A comparative review. *arXiv preprint arXiv:2401.10370*, 2024.
- [3] Adil Rengim Cetingoz and Charles-Albert Lehalle. Synthetic data for portfolios: A throw of the dice will never abolish chance. *arXiv e-prints*, pages arXiv–2501, 2025.
- [4] Julio Backhoff-Veraguas, Daniel Bartl, Mathias Beiglböck, and Manu Eder. Adapted wasserstein distances and stability in mathematical finance. *Finance and Stochastics*, 24:601–632, 2020.
- [5] Jocelyne Bion-Nadal. Time consistent dynamic risk processes. *Stochastic Processes and their Applications*, 119(2):633–654, 2009.
- [6] Martin Glanzer, Georg Ch Pflug, and Alois Pichler. Incorporating statistical model error into the calculation of acceptability prices of contingent claims. *Mathematical Programming*, 174(1):499–524, 2019.
- [7] Daniel Bartl and Johannes Wiesel. Sensitivity of multiperiod optimization problems with respect to the adapted wasserstein distance. *SIAM Journal on Financial Mathematics*, 14(2):704–720, 2023.
- [8] Alois Pichler and Michael Weinhardt. The nested sinkhorn divergence to learn the nested distance. *Computational Management Science*, 19(2):269–293, 2022.
- [9] Stephan Eckstein and Gudmund Pammer. Computational methods for adapted optimal transport. *The Annals of Applied Probability*, 34(1A):675–713, 2024.
- [10] Erhan Bayraktar and Bingyan Han. Fitted value iteration methods for bicausal optimal transport. *arXiv preprint arXiv:2306.12658*, 2023.
- [11] Georg Ch Pflug and Alois Pichler. *Multistage stochastic optimization*, volume 1104. Springer, 2014.
- [12] Beatrice Acciaio, Julio Backhoff-Veraguas, and Anastasiiia Zalashko. Causal optimal transport and its links to enlargement of filtrations and continuous-time stochastic optimization. *Stochastic Processes and their Applications*, 130(5):2918–2953, 2020.
- [13] Beatrice Acciaio, Stephan Eckstein, and Songyan Hou. Time-causal vae: Robust financial time series generator. *arXiv preprint arXiv:2411.02947*, 2024.
- [14] Julio Backhoff, Daniel Bartl, Mathias Beiglböck, and Johannes Wiesel. Estimating processes in adapted wasserstein distance. *The Annals of Applied Probability*, 32(1):529–550, 2022.
- [15] Nicolas Fournier and Arnaud Guillin. On the rate of convergence in wasserstein distance of the empirical measure. *Probability Theory and Related Fields*, 162(3):707–738, 2015.
- [16] Rémi Flamary, Nicolas Courty, Alexandre Gramfort, Mokhtar Z Alaya, Aurélie Boisbunon, Stanislas Chambon, Laetitia Chapel, Adrien Corenflos, Kilian Fatras, Nemo Fournier, et al. Pot: Python optimal transport. *Journal of Machine Learning Research*, 22(78):1–8, 2021.
- [17] Julio Backhoff-Veraguas, Mathias Beiglböck, Yiqing Lin, and Anastasiiia Zalashko. Causal transport in discrete time and applications. *SIAM Journal on Optimization*, 27(4):2528–2562, 2017.
- [18] Beatrice Acciaio and Songyan Hou. Convergence of adapted empirical measures on \mathbb{R}^d . *The Annals of Applied Probability*, 34(5):4799–4835, 2024.
- [19] Asuka Takatsu. On wasserstein geometry of gaussian measures. *Probabilistic approach to geometry*, 57:463–472, 2010.

- [20] Madhu Gunasingam and Ting-Kam Leonard Wong. Adapted optimal transport between gaussian processes in discrete time. *Electronic Communications in Probability*, 30:1–14, 2025.
- [21] Beatrice Acciaio, Songyan Hou, and Gudmund Pammer. Entropic adapted wasserstein distance on gaussians. *arXiv preprint arXiv:2412.18794*, 2024.
- [22] Daniel Bartl, Mathias Beiglböck, and Gudmund Pammer. The wasserstein space of stochastic processes. *Journal of the European Mathematical Society*, 2024.

A Technical Appendices and Supplementary Material

A.1 Notations

We regard \mathbb{R}^{dT} as the space of d -dimensional discrete-time paths with T time steps, $x = (x_1, \dots, x_T)$, equipped with the Euclidean norm $\|\cdot\|$. To refer to the subpath (x_s, \dots, x_t) of x we also write $x_{s:t}$. Moreover, for $\mu \in \mathcal{P}(\mathbb{R}^{dT})$, we denote the t -th marginal of μ by μ_t , the up-to-time- t marginal of μ by $\mu_{1:t}$, and the conditional law of μ conditional on $x_{1:t}$ by $\mu_{x_{1:t}}$, so that the following disintegration holds: $\mu(dx_{1:T}) = \mu_{1:t}(dx_{1:t}) \circ \mu_{x_{1:t}}(dx_{t+1:T})$. To denote the x_s -marginal of $\mu_{x_{1:t}}$ for $s > t$, we use the notation $\mu_{x_{1:t}}^s(dx_s) = (x_{t+1:T} \mapsto x_s) \# \mu_{x_{1:t}}(dx_s)$, where $\#$ designates the push-forward operation. For notational completeness, we let $\mu_{x_{1:0}} = \mu$ where $x_{1:0}$ is a dummy variable. For $\mu, \nu \in \mathcal{P}(\mathbb{R}^{dT})$, we denote their set of couplings by $\text{Cpl}(\mu, \nu) = \{\pi \in \mathcal{P}(\mathbb{R}^{dT} \times \mathbb{R}^{dT}) : \pi(dx \times \mathbb{R}^{dT}) = \mu(dx), \pi(\mathbb{R}^{dT} \times dy) = \nu(dy)\}$, and for every coupling π we use the analogous notations $\pi_{1:t}, \pi_{x_{1:t}, y_{1:t}}, \pi_{x_{1:t}, y_{1:t}}^s, \pi_{x_{1:0}, y_{1:0}}$.

A.2 Robustness

Optimal stopping: Let $f: \mathbb{R}^d \times \{1, \dots, T\} \rightarrow \mathbb{R}$ bounded and consider the optimal stopping problem:

$$v(\mu) = \sup_{\tau \in \mathcal{T}} \mathbb{E}_{X \sim \mu}[f(X_\tau, \tau)],$$

where \mathcal{T} is the set of bounded optimal stopping time adapted to the natural filtration; see [12, Proposition 4.4] and [7, Theorem 2.8].

Utility maximization: Let $\ell: \mathbb{R} \rightarrow \mathbb{R}$ be a convex loss function, i.e., ℓ is bounded from below and convex. Moreover let $g: \mathbb{R}^T \rightarrow \mathbb{R}$ be (the negative of) a payoff function and consider the problem:

$$v(\mu) := \inf_{a \in \mathcal{A}} \mathbb{E}_{X \sim \mu} \left[\ell \left(g(X) + \sum_{t=1}^{T-1} a_{t+1}(X)(X_{t+1} - X_t) \right) \right],$$

where \mathcal{A} denotes the set of all *predictable controls* bounded by L , i.e., every $a = (a_t)_{t=1}^T \in \mathcal{A}$ is such that $a_t: \mathbb{R}^T \rightarrow \mathbb{R}$ only depends on $x_{1:t-1}$ and that $|a_t| \leq B$ for a fixed constant B ; see [12, Proposition 4.8] and [7, Corollary 2.7].

Risk minimization: Let $\text{AVaR}_\alpha^\mu(\cdot)$ be the Average Value at Risk (or Expected Shortfall) at confidence level $\alpha > 0$ under μ , and consider the problem:

$$v(\mu) := \inf_{a \in \mathcal{A}} \text{AVaR}_\alpha^\mu \left(\sum_{t=1}^{T-1} a_{t+1}(X)(X_{t+1} - X_t) \right),$$

where \mathcal{A} is defined as above; see [11, Corollary 6.9] and [13, Corollary 3.4].

A.3 Proofs.

Proof of Proposition 1. The proof follows directly from [17, Proposition 5.2] by taking the cost function $c(x, y) = \sum_{t=1}^T \|x_t - y_t\|^2$. \square

Proof of Theorem 2. Since $\mu \in \mathcal{P}_2(\mathbb{R}^{dT})$ implies $\mu \in \mathcal{P}_1(\mathbb{R}^{dT})$, then by Theorem 2.7 in [18], we prove the almost sure convergence. \square

A.4 Closed-form for Gaussians

For Gaussian distributions, closed-form have been established for both \mathcal{AW}_2 -distance and \mathcal{W}_2 -distance.

Theorem 3 (Theorem 2.2 in [19]). *Let $\mu = \mathcal{N}(a, A)$ and $\nu = \mathcal{N}(b, B)$ be non-degenerate Gaussians on \mathbb{R}^T . Then*

$$\mathcal{W}_2^2(\mu, \nu) = |a - b|^2 + \text{tr}\left(A + B - 2\left(A^{\frac{1}{2}}BA^{\frac{1}{2}}\right)^{\frac{1}{2}}\right). \quad (3)$$

Theorem 4 (Theorem 1.1 in [20]). *Let $\mu = \mathcal{N}(a, A)$ and $\nu = \mathcal{N}(b, B)$ be non-degenerate Gaussians on \mathbb{R}^T , whose covariance matrices have Cholesky decompositions $A = LL^\top$ and $B = MM^\top$. Then*

$$\mathcal{AW}_2^2(\mu, \nu) = |a - b|^2 + \text{tr}(LL^\top + MM^\top - 2|M^\top L|). \quad (4)$$

For d -dimensional Gaussian processes with T time steps and $d > 1$, the \mathcal{W}_2 -distance follows the same closed form as \mathcal{W}_2 -distance is regardless of time structure, while the close-form of \mathcal{AW}_2 -distance is slightly different from the $d = 1$ case.

Theorem 5 (Theorem 2.2 in [21]). *Let $\mu = \mathcal{N}(a, A)$ and $\nu = \mathcal{N}(b, B)$ be non-degenerate Gaussians on \mathbb{R}^{dT} , whose covariance matrices have Cholesky decompositions $A = LL^\top$ and $B = MM^\top$. Then*

$$\mathcal{AW}_2^2(\mu, \nu) = |a - b|^2 + \text{tr}(LL^\top + MM^\top) - 2\text{tr}(S), \quad (5)$$

where $S = \text{diag}(S_1, \dots, S_T)$, with S_t being the diagonal matrix of singular values of $(M^\top L)_{t,t}$.

When the marginal μ is degenerate, the Cholesky decomposition is not unique. Different choice of Cholesky decomposition leads to different \mathcal{AW} -distances. This might sounds weird at the first glance. However, if you see different Cholesky decomposition characterizing different filtration structure, this totally make sense for stochastic process. For example, $L = \begin{bmatrix} 0 & 0 \\ 1 & 1 \end{bmatrix}$ and $M = \begin{bmatrix} 0 & 0 \\ 0 & \sqrt{2} \end{bmatrix}$ lead to

the same Gaussian distribution because $LL^\top = MM^\top$. However, from a stochastic process point of view, they are indeed different. Let $G \sim \mathcal{N}(0, I_2)$ be a noise process and define two processes: $X = LG$ and $Y = MG$. Let $\mathcal{F}_t = \sigma(G_{1:t})$, $t = 1, 2$ the natural filtration generated by the noise process. Then $Y_2 = \sqrt{2}G_2$ is independent of \mathcal{F}_1 while this is not the case for $X_2 = G_1 + G_2$. This argument is formally addressed by extending \mathcal{AW} -distance to *filtered processes* \mathcal{FP} in [22], where $(\mathcal{FP}, \mathcal{AW})$ builds a geodesic space, which is isometric to a classical Wasserstein space. Under the filtered process setting, Gaussian process are characterized uniquely by the Cholesky decomposition instead of covariance matrix, and by following the same proof in [21], the closed-form of (4) and (5) generalizes to degenerate Gaussian distributions.